AJNR

Impact of Model-Based Iterative Reconstruction on Image Quality of Contrast-Enhanced Neck CT

S. Gaddikeri, J.B. Andre, J. Benjert, D.S. Hippe and Y. Anzai

This information is current as of April 26, 2024.

Impact of Model-Based Iterative Reconstruction on Image Quality of Contrast-Enhanced Neck CT

S. Gaddikeri, J.B. Andre, J. Benjert, D.S. Hippe, and Y. Anzai

ABSTRACT

BACKGROUND AND PURPOSE: Improved image quality is clinically desired for contrast-enhanced CT of the neck. We compared 30% adaptive statistical iterative reconstruction and model-based iterative reconstruction algorithms for the assessment of image quality of contrast-enhanced CT of the neck.

MATERIALS AND METHODS: Neck contrast-enhanced CT data from 64 consecutive patients were reconstructed retrospectively by using 30% adaptive statistical iterative reconstruction and model-based iterative reconstruction. Objective image quality was assessed by comparing SNR, contrast-to-noise ratio, and background noise at levels 1 (mandible) and 2 (superior mediastinum). Two independent blinded readers subjectively graded the image quality on a scale of 1–5, (grade 5 = excellent image quality without artifacts and grade 1 = nondiagnostic image quality with significant artifacts). The percentage of agreement and disagreement between the 2 readers was assessed.

RESULTS: Compared with 30% adaptive statistical iterative reconstruction, model-based iterative reconstruction significantly improved the SNR and contrast-to-noise ratio at levels 1 and 2. Model-based iterative reconstruction also decreased background noise at level 1 (P = .016), though there was no difference at level 2 (P = .61). Model-based iterative reconstruction was scored higher than 30% adaptive statistical iterative reconstruction by both reviewers at the nasopharynx (P < .001) and oropharynx (P < .001) and for overall image quality (P < .001) and was scored lower at the vocal cords (P < .001) and sternoclavicular junction (P < .001), due to artifacts related to thyroid shielding that were specific for model-based iterative reconstruction.

CONCLUSIONS: Model-based iterative reconstruction offers improved subjective and objective image quality as evidenced by a higher SNR and contrast-to-noise ratio and lower background noise within the same dataset for contrast-enhanced neck CT. Model-based iterative reconstruction has the potential to reduce the radiation dose while maintaining the image quality, with a minor downside being prominent artifacts related to thyroid shield use on model-based iterative reconstruction.

ABBREVIATIONS: ASiR30 = 30% adaptive statistical iterative reconstruction; BN = background noise; CNR = contrast-to-noise ratio; FBP = filtered back-projection; HU, Hounsfield units; MBIR = model-based iterative reconstruction; PM = pectoris muscle; SCM = sternocleidomastoid muscle; SVC = superior vena cava

Since the introduction of CT for medical imaging in the early 1970s, there has been tremendous advancement in overall image quality with concomitant shortening of requisite scan times.

Additional major effort has been undertaken to reduce the radiation dose to improve patient safety while maintaining image quality. In particular, image reconstruction algorithms have evolved from the traditional analytic algorithms such as filtered back-projection (FBP) to newer iterative reconstruction methods such as adaptive statistical iterative reconstruction (ASiR; GE Healthcare, Milwaukee, Wisconsin) and most recently model-based iterative reconstruction (MBIR; GE Healthcare), which models system noise statistics and optics.

Both phantom and clinical studies have confirmed that the application of the MBIR algorithm results in an improved contrast-to-noise ratio (CNR), lower background noise (BN),[1-4] and reduction of helical conebeam artifacts.[2,4] Clinical studies in the delineation of arteries in the posterior fossa on 3D brain CT angiography,[1] improved liver lesion detection,[3,5] general evaluation

Table 1: Soft-tissue neck CT protocol

CT Protocol	
Scanned region	1 cm above the level of frontal sinus to aortopulmonary window
Type	Helical 0.5-second duration.
Pitch	0.984:1
Gantry tilt	0°
Section thickness and section interval	0.625-mm-thick/0.625 interval and 40-mm detector coverage
Reconstruction	Standard soft-tissue algorithm with 2.5-mm thickness
Matrix	512 × 512
Kilovolt(peak)	140
Noise index at 0.625-mm section thickness	40 HU

iohexol, 350 mg/mL (Omnipaque 350; GE Healthcare), was intravenously administered via a power injector (the initial 50 mL at a rate of 2 mL/s and the remaining 30 mL at 0.5 mL/s) followed by 30 mL of saline (0.9% NaCl) flush at a rate of 1.5 mL/s. The scan was acquired with a delay of 120 seconds following the commencement of contrast injection. A bismuth thyroid shield was placed over the lower neck in all patients as part of a radiation safety exercise at our institution.[8]

FIG 1. Assessment of objective image quality at the level of the mandible (*A*) and superior mediastinum (*B*). Region of interest drawn to measure the SD of air bilaterally (background noise), attenuation of the sternocleidomastoid and pectoralis major muscles, internal jugular vein and superior vena cava, and surrounding fat for the estimation of signal-to-noise ratio and contrast-to-noise ratio.

of abdominopelvic CT,[2] and pediatric chest CT[6] all support the use of MBIR, with or without radiation-dose reduction. In this study, we compared objective and subjective image quality in neck CT images reconstructed with 2 different iterative reconstruction algorithms (MBIR versus 30% adaptive statistical iterative reconstruction [ASiR30]) by using the same raw dataset.

MATERIALS AND METHODS
Patients
The local institutional review board approved this Health Insurance Portability and Accountability Act–compliant retrospective study. Sixty-four consecutive contrast-enhanced CT neck examinations, performed during June and July 2013, were included in this study. There were 42 male (66%) and 22 female (34%) patients (median age, 61 years; age range, 20–84 years). The indications for neck CT examinations included initial head and neck cancer staging, lymphoma staging and surveillance, routine follow-up in the setting of treated tumor, and known or suspected soft-tissue neck infection.

Neck CT Protocol
Details of the contrast-enhanced CT neck protocols are described in Table 1. All CT examinations were performed on a 64−detector row multidetector CT (Discovery HD 75; GE Healthcare), with tube current modulation applied at a noise index of 40 Hounsfield units (HU) for 0.625-mm section thickness by using 0.5-second helical gantry rotation. Because the noise index varies with the section thickness, the predicted noise index for 2.5-mm section thickness was about 23.4 HU.[7] For each diagnostic scan, 80 mL of

CT Data Reconstruction
The raw data from each subject's CT examination were reconstructed at the scanner, with a similar magnification, 2.5-mm section thickness at an interval of 2.5 mm in the axial plane, first with ASiR30 and then with MBIR. Details regarding specifically used reconstruction methods were omitted from the generated image sets to ensure complete blinding of the subjective imaging review. The images were sent to the PACS for analysis.

Quantitative Image Analysis
Quantitative image parameters were assessed by a neuroradiologist with a cumulative experience of 8 years (including 2 years of fellowship training in neuroradiology) in interpreting neck CT examinations (S.G.). Several region-of-interest measurements were performed on a PACS workstation by using a 0.5- to 10-mm-diameter circle tool. Mean attenuation values (V) and SD were measured and recorded in Hounsfield units. BN was also measured and recorded as the SD of air. The measurements on each image set were performed at 2 anatomic levels: level 1, the angle of the mandible (Fig 1*A*) and level 2, the superior mediastinum (Fig 1*B*). BN was assessed bilaterally at each level, and the mean was calculated. We placed ROIs on the following structures and recorded their respective measurements: The sternocleidomastoid muscle (SCM) (level 1), pectoralis major muscle (PM) (level 2), dominant internal jugular vein (level 1), superior vena cava (SVC) (level 2), and the surrounding fat (both levels) were measured. Signal-to-noise ratio and the CNR were calculated by using the following standard equations[9]:

$$SNR = V_{\mathrm{muscle}}/BN,$$

$$CNR = V_{\mathrm{vein}} - V_{\mathrm{muscle}}/[(SD_{\mathrm{vein}})^2 + (SD_{\mathrm{muscle}})^2]^{1/2}.$$

Qualitative Image Analysis
Qualitative image analysis was performed at 4 predefined anatomic levels: 1) the nasopharynx (at the level of fossa of Rosenmuller); 2) the oropharynx (at the level of palatine tonsils); 3) the true vocal cords, and 4) the sternoclavicular junction. In patients with prior tonsillectomy or laryngectomy, images were selected at the level of the surgical bed. On a per-subject basis, identical anatomic levels were selected carefully from both the ASiR30 and MBIR image sets. These 4 anatomic levels were specifically chosen for their increased respective incidence of head and neck cancers and/or a proclivity for streak (due to dental amalgam) or beam-

Table 2: Quantitative assessment of image quality (N = 64 subjects)

	MBIR		ASiR		Difference (MBIR-ASiR)		
	Mean	(95% CI)	Mean	(95% CI)	Mean	(95% CI)	P Value[a]
Level 1 (angle of mandible)							
Mean of IJV (HU)	130.3 ± 19.6	(125.4–135.1)	131.0 ± 19.2	(126.2–135.8)	−0.7 ± 2.7	(−1.4 to −0.1)	.030
Mean of SCM (HU)	62.9 ± 5.0	(61.7–64.2)	64.4 ± 4.9	(63.2–65.6)	−1.5 ± 2.2	(−2.0 to −0.9)	<.001
Mean of fat (HU)	−81.4 ± 23.2	(−87.2 to −75.6)	−77.1 ± 23.3	(−82.9 to −71.3)	−4.2 ± 8.1	(−6.3 to −2.2)	<.001
SD of IJV (HU)	6.3 ± 2.6	(5.7–7.0)	7.3 ± 2.0	(6.8–7.8)	−1.0 ± 1.9	(−1.5 to −0.6)	<.001
SD of SCM (HU)	6.6 ± 1.4	(6.3–7.0)	7.1 ± 1.6	(6.7–7.5)	−0.5 ± 1.5	(−0.8 to −0.1)	.020
SD of air (BN) (HU)	6.3 ± 9.2	(4.0–8.6)	7.8 ± 9.2	(5.5–10.1)	−1.5 ± 4.8	(−2.7 to −0.3)	.016
SNR of SCM	16.2 ± 7.2	(14.4–18.0)	12.1 ± 4.3	(11.0–13.2)	4.1 ± 5.7	(2.7–5.5)	<.001
CNR of IJV and SCM	7.6 ± 2.6	(7.0–8.3)	6.8 ± 2.4	(6.2–7.4)	0.9 ± 1.4	(0.5–1.2)	<.001
Lower level 2 (superior mediastinum)							
Mean of SVC (HU)	119.8 ± 24.5	(113.7–125.9)	117.8 ± 23.7	(111.8–123.7)	2.0 ± 7.3	(0.2–3.9)	.030
Mean of PM (HU)	55.6 ± 11.0	(52.9–58.4)	53.3 ± 13.0	(50.1–56.5)	2.3 ± 7.9	(0.4–4.3)	.021
Mean of fat (HU)	−101.3 ± 19.4	(−106.2 to −96.5)	−98.9 ± 18.1	(−103.4 to −94.3)	−2.5 ± 7.7	(−4.4 to −0.6)	.012
SD of SVC (HU)	10.2 ± 4.5	(9.1–11.3)	13.7 ± 4.9	(12.5–14.9)	−3.5 ± 2.8	(−4.2 to −2.8)	<.001
SD of PM (HU)	8.5 ± 2.4	(7.9–9.1)	10.9 ± 2.9	(10.2–11.6)	−2.4 ± 3.0	(−3.2 to −1.7)	<.001
SD of air (BN) (HU)	32.1 ± 32.5	(23.9–40.2)	33.5 ± 30.5	(25.9–41.1)	−1.4 ± 23	(−7.1–4.2)	.61
SNR of PM	6.9 ± 8.1	(4.9–9.0)	3.9 ± 3.4	(3.0–4.7)	3.1 ± 6.4	(1.5–4.7)	<.001
CNR of SVC and PM	4.9 ± 2.0	(4.4–5.4)	3.7 ± 1.6	(3.3–4.1)	1.2 ± 1.3	(0.9–1.5)	<.001

Note:—IJV indicates internal jugular vein.
[a] Paired *t* test.

hardening (due to shoulders) artifacts. In addition, readers subjectively evaluated all the images within an image stack (ASiR30 versus MBIR) to assess overall image quality.

Two experienced fellowship-trained neuroradiologists with 9 (J.B. [reader 1]) and 10 (J.B.A. [reader 2]) years of cumulative experience in interpreting neck CT examinations were blinded to the patient information and reconstruction methodology. On a per-patient basis, image stacks obtained from the 2 reconstruction algorithms were displayed side-by-side on each of 2 PACS monitors. Images were presented to reviewers with a prespecified window width and level of 350 and 50 HU, respectively, though reviewers were free to vary both at their discretion. In the absence of a focal lesion, the readers (1 and 2) were asked to evaluate the appearance of normal structures, with special attention paid to the delineation of fat planes, the internal architecture of soft tissues, and overall artifacts burden. In the presence of a focal lesion, readers were asked to evaluate lesion conspicuity, the margins, internal architecture of the lesion, and overall artifacts burden.

Overall image quality and image quality at each of the 4 preselected anatomic locations were graded on a scale of 1–5 (5 = excellent, no artifacts; 4 = good, minimal artifacts; 3 = acceptable, mild artifacts; 2 = suboptimal, moderate artifacts; and 1 = nondiagnostic, significant artifacts). Grades 1 and 2 were considered unacceptable for clinical interpretation. On the basis of the grades of qualitative assessment by each of the readers (1 and 2), the data were divided into 2 categories: category I (readers agree that ASiR>MBIR) and category II (readers agree that MBIR≥ASiR).

Statistical Analysis

The paired Student *t* test was used to assess differences in objective measures of image quality between the 2 reconstruction algorithms. Histograms were visually inspected to ensure that distributional assumptions were reasonable. The Wilcoxon signed rank test was used to test for differences in subjective image-quality ratings between the 2 reconstruction algorithms and readers. The percentage agreement of the 2 readers (1 and 2) for the categories I (readers agree that ASiR>MBIR) or II (readers agree that MBIR≥ASiR) was assessed at all 4 levels and for overall image

quality. All statistical calculations were conducted with the statistical computing language R (R statistical computing software; (http://www.r-project.org/). Throughout, 2-tailed tests were used with P < .05 denoting statistical significance.

RESULTS

Quantitative Analysis

Objective image-quality measurement data are summarized in Table 2. At level 1, the mean BN was significantly lower (P = .016) for MBIR compared with ASiR30. The mean attenuation values of the internal jugular vein and SCM for the MBIR dataset were significantly lower (P = .03 and P < .001, respectively) in comparison with the ASiR30 dataset. At level 2, there was no statistically significant difference (P = .61) in the BN between the MBIR and ASiR30 image sets, whereas the mean attenuation values of SVC and PM for the MBIR dataset were significantly higher (P = .03 and P < .021, respectively) compared with the ASiR30 dataset.

The measured SNRs of the SCM and PM were significantly higher (P < .001 and P < .001, respectively) for the MBIR dataset compared with the ASiR30 dataset, likely due to reduced BN. The measured CNR of the internal jugular vein and SVC in relation to the SCM and PM was also significantly higher (P < .001 and P < .001, respectively) for MBIR compared with ASiR30.

Qualitative Analysis

Subjective image-quality assessment is summarized in Table 3. Both readers preferentially graded MBIR over ASiR30 for overall image quality (the entire stack of images) (P < .001) and at the levels of the nasopharynx and oropharynx (Figs 2 and 3). Readers preferentially graded ASiR30 over MBIR (P < .001) at the level of the vocal cords and sternoclavicular region (Fig 4).

The percentage of agreement and disagreement between the readers for categories I and II is presented as a bar graph (Fig 5). Reader agreement in preferring MBIR to ASiR30 was 83% for overall image quality, 100% at the level of nasopharynx, and 98% at the level of the oropharynx. The percentage of agreement between the 2 readers at the level of the vocal cords and sternoclavicular junction, however, was only 41% and 42%, respectively.

**Table 3: Qualitative assessment of image quality, based on average ratings of 2 readers (N = 64 subjects)**

	MBIR		ASiR		Difference (MBIR-ASiR)		
	Mean	(95% CI)	Mean	(95% CI)	Mean	(95% CI)	P Value[a]
Nasopharynx	4.80 ± 0.26	(4.74–4.87)	4.16 ± 0.31	(4.08–4.23)	0.65 ± 0.30	(0.57–0.72)	<.001
Oropharynx	3.74 ± 0.60	(3.59–3.89)	3.08 ± 0.64	(2.92–3.24)	0.66 ± 0.37	(0.56–0.75)	<.001
Vocal cord	3.73 ± 0.53	(3.59–3.86)	4.02 ± 0.37	(3.92–4.11)	−0.29 ± 0.53	(−0.42 to −0.16)	<.001
SC junction	3.41 ± 0.48	(3.29–3.53)	3.75 ± 0.25	(3.69–3.82)	−0.34 ± 0.52	(−0.47 to −0.21)	<.001
Overall IQ	3.85 ± 0.32	(3.77–3.93)	3.69 ± 0.28	(3.62–3.76)	0.17 ± 0.31	(0.09–0.24)	<.001

Note:—SC indicates sternoclavicular; IQ, image quality.
[a] Wilcoxon signed ranked test.
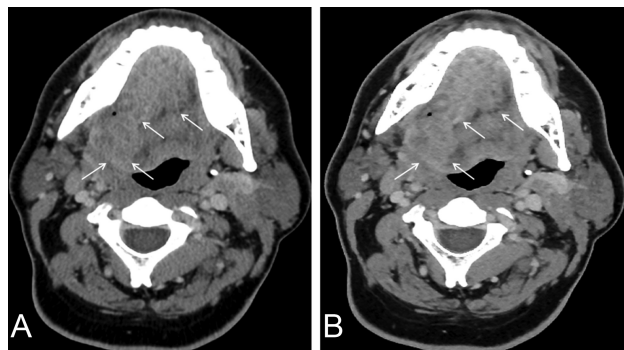
FIG 2. Axial images of contrast-enhanced neck CT at the level of oropharynx reconstructed by using 30% adaptive statistical iterative reconstruction (*A*) and model-based iterative reconstruction (*B*). Note better conspicuity and definition of tumor margins on MBIR (*arrows*) compared with ASiR30 (*arrows*).
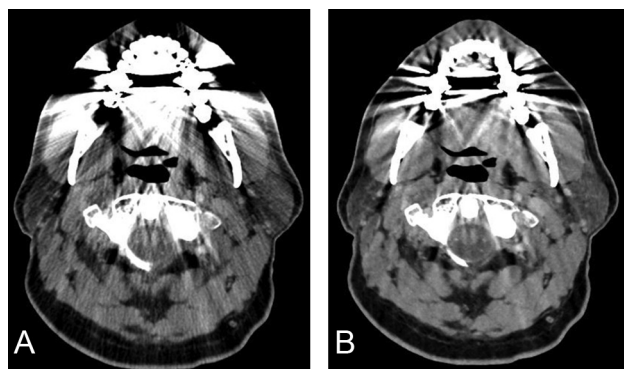
FIG 3. Axial images of contrast-enhanced neck CT at the level of oropharynx reconstructed by using 30% adaptive statistical iterative reconstruction (*A*) and model-based iterative reconstruction (*B*). Note a decrease in the streak artifacts related to dental amalgam particularly in the region of the base of the tongue, parotids, and foramen magnum and a poorer definition of fat planes in the parapharyngeal space on MBIR images.

DISCUSSION

CT, enabled by technologic advances and widespread availability, has become the imaging technique of choice in the assessment of numerous neck pathologies. Multidetector CT technology has brought a commensurate increase in the number of CT studies performed,[10] leading to a significant increase in the radiation dose related to CT scanning.[11,12] Although CT scanning is only approximately 15% of all radiologic examinations, it accounts for up to 70% of the radiation dose to the patient.[13] Increasing media attention and public awareness regarding the potential risks of radiation exposure, particularly radiation-induced carcinogenesis, have encouraged development of strategies to further reduce the patient radiation dose. The radiation risk to children is of particular concern because the estimated lifetime

cancer risk for a 1-year-old child from the radiation exposure of a head CT is 0.07%.[14] Radiation-induced carcinogenesis may be related to a linear no-threshold stochastic effect[15] or a cumulative radiation effect,[16] particularly in patients with a known history of cancer or other chronic head and neck diseases warranting repeat CT imaging.

There are several strategies for radiation-dose reduction in clinical CT examinations, including changing the CT acquisition parameters (tube current, tube rotation time, peak voltage, pitch, and collimation), use of tube current modulation,[17] automatic exposure control,[18] adjusting the kV on the basis of patient size,[19] iterative reconstruction,[20-22] and selective in-plane shielding[23] (thyroid, eye lens, breast, or gonadal shield). Developing appropriate CT protocols with an optimal compromise between diagnostic image quality and radiation dose is a team effort of technologist, physicist, and radiologist.[24]

The FBP algorithm for CT image reconstruction has been the preferred reconstruction algorithm for CT images since its introduction in the 1970s. FBP is based on the assumption that the CT system is perfect and noise-free. However, FBP actually amplifies the quantum and electronic noise in the projection data.[25] Its main advantages include speed of image reconstruction due to single-pass direct calculation and production of CT images that are routinely considered clinically acceptable. To overcome the limitation of analytic FBP, iterative techniques for image reconstruction were introduced. ASiR (GE Healthcare) is a partially iterative method using a statistical model of noise that has been commercially available since 2008.[20,21] It uses the information obtained by initial FBP reconstruction and then repeatedly compares the estimated pixel value with the ideal value predicted by the noise model, until the estimated and ideal values converge.[26]

MBIR is a fully iterative method that not only models the statistics of noise (photon statistic and electronic noise) but additionally models the system optics (detector response to incident x-ray beam).[4,27] Prior research has suggested that the MBIR algorithm generates CT images with better noise suppression, spatial resolution, conspicuity, and overall image quality compared with FBP, while maintaining similar uniformity and beam-hardening.[28] Several studies have reported clinically relevant radiation-dose reduction by using MBIR while still preserving diagnostic image quality.[2,5,6,25] One notable drawback of the current version of the MBIR is that it can only reconstruct CT images by using a standard soft-tissue kernel and not a bone kernel; hence, this algorithm fails to provide images with requisite edge details for better assessment of bony lesions.

In this study, the neck CT images reconstructed by using MBIR showed significantly improved SNR and CNR while reduc-
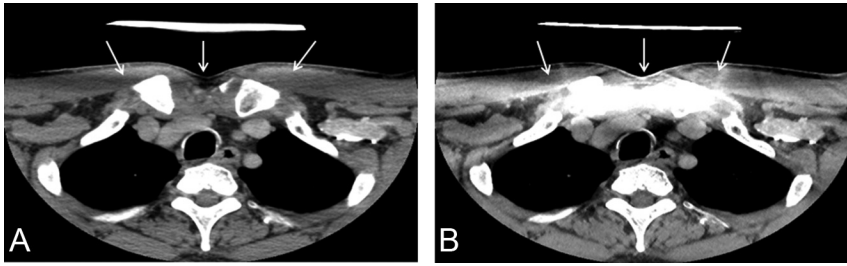
FIG 4. Axial images of contrast-enhanced neck CT at the level of sternoclavicular junction reconstructed by using 30% adaptive statistical iterative reconstruction (*A*) and model-based iterative reconstruction (*B*). Artifacts are due to a thyroid shield in the display FOV specific for MBIR (*arrows*). Note the absence of these thyroid shield artifacts on images reconstructed by using ASiR30 (*arrows*).
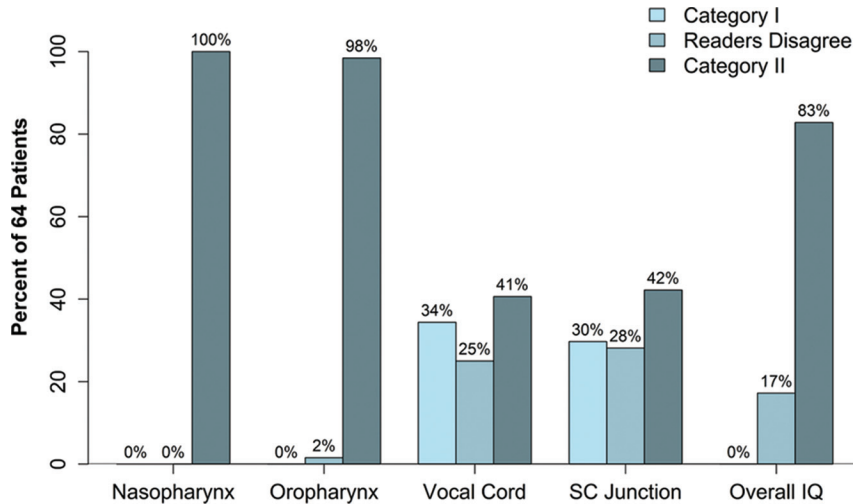
FIG 5. Bar graph showing the percentage of agreement and disagreement between the 2 independent readers (1 and 2) for the assessment of subjective image quality at various levels and overall image quality in both categories (category I: ASiR>MBIR and category II: MBIR≥ASiR).

clude further improvement in CNR, decrease in BN, and decrease in artifacts while preserving the diagnostic image quality.[1-3,5,6] In this study, overall image quality in neck CT examinations was improved with MBIR, potentially allowing the exchange of improved image quality for further radiation-dose reduction. A recent study applying MBIR to chest CT reported radiation-dose reductions approaching 70%–80%.[16] In contrast, the expected dose reduction from using a bismuth thyroid shield is 28%.[8] If a similar radiation-dose reduction can be achieved in contrast-enhanced neck CT examinations by applying a particular postprocessing algorithm, then one could argue that the use of a thyroid shield is less warranted.

The main drawback of MBIR in its present form over other reconstruction algorithms is the computing time, which is about 1 image per second as opposed to 15 images per second for FBP and 10 images per second for ASiR50. In our study, the average reconstruction time for individual soft-tissue neck CT examinations was approximately 45 minutes (range, 30–75 minutes). This time constraint for MBIR, however, should be reduced in the near future due to advancements in computational power.

ing the BN compared with images reconstructed by using ASiR30. The qualitative assessment by 2 blinded independent readers suggests that MBIR is superior to ASiR30 at the levels of nasopharynx and oropharynx. However, qualitative assessment at the levels of the vocal cords and sternoclavicular region suggests that ASiR30 is preferred over MBIR in these regions. This observation may, in part, be explained by the presence of a bismuth thyroid shield used for radiation-dose reduction to the thyroid gland. The bismuth shield resulted in artifacts projecting over the vocal cords and sternoclavicular region, which was more prominent on images reconstructed with MBIR, particularly when the shield was close to the skin surface. The exact cause of these artifacts in CT images reconstructed with the MBIR algorithm remains unknown, though we believe that it is at least partly related to the current noise model of the MBIR algorithm, which is not well-equipped to deal with the sharp changes in local attenuation and statistics in the projection sinogram produced at the edges of the bismuth shield. We also believe that these thyroid shield artifacts contributed to the underperformance of MBIR at the level of the vocal cords and sternoclavicular region.

It has been reported from various clinical studies that MBIR methods are better than analytic FBP and ASiR algorithms in providing acceptable image quality in the setting of a lower radiation dose.[1-3,29-31] The major advantages of MBIR over ASiR in-

Study Limitations

Our study has many limitations. First, we did not perform a quality comparison of the MBIR image algorithm with and without the use of a thyroid shield to more accurately compare the image quality of ASiR and MBIR. Second, the qualitative image analysis was a simultaneous assessment of image quality and artifacts burden. As such, this may explain lower subjective scores in areas covered by the thyroid shield. Third, patient data collection was performed in a consecutive fashion, without discrete inclusion criteria to evaluate a specific pathology; thus our study cannot assess the impact of MBIR on the detection of disease.

CONCLUSIONS

MBIR offers improved subjective and objective image quality for contrast-enhanced neck CT, suggesting that MBIR may further reduce the radiation dose while maintaining diagnostic image quality. Further studies are necessary to assess how much radiation-dose savings can be achieved with the application of newer and faster model-based iterative reconstruction algorithms, and further development will be required to bring image processing into clinically reasonable timeframes.

REFERENCES

1. Machida H, Takeuchi H, Tanaka I, et al. **Improved delineation of arteries in the posterior fossa of the brain by model-based iterative reconstruction in volume-rendered 3D CT angiography.** *AJNR Am J Neuroradiol* 2013;34:971–75

2. Yasaka K, Katsura M, Akahane M, et al. **Model-based iterative reconstruction for reduction of radiation dose in abdominopelvic CT: comparison to adaptive statistical iterative reconstruction.** *Springerplus* 2013;2:209

3. Shuman WP, Green DE, Busey JM, et al. **Model-based iterative reconstruction versus adaptive statistical iterative reconstruction and filtered back projection in liver 64-MDCT: focal lesion detection, lesion conspicuity, and image noise.** *AJR Am J Roentgenol* 2013;200:1071–76

4. Thibault JB, Sauer KD, Bouman CA, et al. **A three-dimensional statistical approach to improved image quality for multislice helical CT.** *Med Phys* 2007;34:4526–44

5. Volders D, Bols A, Haspeslagh M, et al. **Model-based iterative reconstruction and adaptive statistical iterative reconstruction techniques in abdominal CT: comparison of image quality in the detection of colorectal liver metastases.** *Radiology* 2013;269:469–74

6. Miéville FA, Berteloot L, Grandjean A, et al. **Model-based iterative reconstruction in pediatric chest CT: assessment of image quality in a prospective study of children with cystic fibrosis.** *Pediatr Radiol* 2013;43:558–67

7. Kanal KM, Stewart BK, Kolokythas O, et al. **Impact of operator-selected image noise index and reconstruction slice thickness on patient radiation dose in 64-MDCT.** *AJR Am J Roentgenol* 2007; 189:219–25

8. Gunn ML, Kanal KM, Kolokythas O, et al. **Radiation dose to the thyroid gland and breast from multidetector computed tomography of the cervical spine: does bismuth shielding with and without a cervical collar reduce dose?** *J Comput Assist Tomogr* 2009; 33:987–90

9. Bodelle B, Bauer RW, Holthaus L, et al. **Dose and image quality of high-pitch dual source computed tomography for the evaluation of cervical lymph node status: comparison to regular 128-slice single source computed tomography.** *Eur J Radiol* 2013;82:e281–285

10. Kalra MK, Maher MM, Toth TL, et al. **Strategies for CT radiation dose optimization.** *Radiology* 2004;230:619–28

11. Wiest PW, Locken JA, Heintz PH, et al. **CT scanning: a major source of radiation exposure.** *Semin Ultrasound CT MR* 2002;23:402–10

12. Imhof H, Schibany N, Ba-Ssalamah A, et al. **Spiral CT and radiation dose.** *Eur J Radiol* 2003;47:29–37

13. Linton OW, Mettler FA Jr. **National conference on dose reduction in CT, with an emphasis on pediatric patients.** *AJR Am J Roentgenol* 2003;181:321–29

14. Brenner D, Elliston C, Hall E, et al. **Estimated risks of radiation-induced fatal cancer from pediatric CT.** *AJR Am J Roentgenol* 2001;176:289–96

15. Sodickson A, Baeyens PF, Andriole KP, et al. **Recurrent CT, cumulative radiation exposure, and associated radiation-induced cancer risks from CT of adults.** *Radiology* 2009;251:175–84

16. Katsura M, Matsuda I, Akahane M, et al. **Model-based iterative reconstruction technique for radiation dose reduction in chest CT: comparison with the adaptive statistical iterative reconstruction technique.** *Eur Radiol* 2012;22:1613–23

17. Greess H, Wolf H, Baum U, et al. **Dose reduction in computed tomography by attenuation-based on-line modulation of tube current: evaluation of six anatomical regions.** *Eur Radiol* 2000; 10:391–94

18. Mulkens TH, Bellinck P, Baeyaert M, et al. **Use of an automatic exposure control mechanism for dose optimization in multi-detector row CT examinations: clinical evaluation.** *Radiology* 2005;237: 213–23

19. McCollough CH, Primak AN, Braun N, et al. **Strategies for reducing radiation dose in CT.** *Radiol Clin North Am* 2009;47:27–40

20. Hara AK, Paden RG, Silva AC, et al. **Iterative reconstruction technique for reducing body radiation dose at CT: feasibility study.** *AJR J Roentgenol* 2009;193:764–71

21. Vachha B, Brodoefel H, Wilcox C, et al. **Radiation dose reduction in soft tissue neck CT using adaptive statistical iterative reconstruction (ASIR).** *Eur J Radiol* 2013;82:2222–26

22. Nuyts J, De Man B, Dupont P, et al. **Iterative reconstruction for helical CT: a simulation study.** *Phys Med Biol* 1998;43:729–37

23. Geleijns J, Salvado Artells M, Veldkamp WJ, et al. **Quantitative assessment of selective in-plane shielding of tissues in computed tomography through evaluation of absorbed dose and image quality.** *Eur Radiol* 2006;16:2334–40

24. Hamberg LM, Rhea JT, Hunter GJ, et al. **Multi-detector row CT: radiation dose characteristics.** *Radiology* 2003;226:762–72

25. Fleischmann D, Boas FE. **Computed tomography: old ideas and new technology.** *Eur Radiol* 2011;21:510–17

26. Silva AC, Lawder HJ, Hara A, et al. **Innovations in CT dose reduction strategy: application of the adaptive statistical iterative reconstruction algorithm.** *AJR J Roentgenol* 2010;194:191–99

27. Yu Z, Thibault JB, Bouman CA, Sauer KD, et al. **Fast model-based X-ray CT reconstruction using spatially nonhomogeneous ICD optimization.** *IEEE Trans Image Process* 2011;20:161–75

28. Gramer BM, Muenzel D, Leber V, et al. **Impact of iterative reconstruction on CNR and SNR in dynamic myocardial perfusion imaging in an animal model.** *Eur Radiol* 2012;22:2654–61

29. Kilic K, Erbas G, Guryildirim M, et al. **Lowering the dose in head CT using adaptive statistical iterative reconstruction.** *AJNR Am J Neuroradiol* 2011;32:1578–82

30. Niu Y, Wang Z, Liu Y, et al. **Radiation dose to the lens using different temporal bone CT scanning protocols.** *AJNR Am J Neuroradiol* 2010;31:226–29

31. Singh S, Kalra MK, Hsieh J, et al. **Abdominal CT: comparison of adaptive statistical iterative and filtered back projection reconstruction techniques.** *Radiology* 2010;257:373–83